Deterministic and Robust Optimization of Hybrid Rocket Engines for Small Satellite Launchers*

Lorenzo Casalino†, Filippo Masseni‡ and Dario Pastrone§
Politecnico di Torino, Torino, Italy 10129

In this paper design and optimization approaches are applied to an hybrid-powered small-satellite launcher, namely a deterministic and a robust-based method. A unique hybrid rocket engine is considered, employed in different numbers in each stage of the three-stage launcher: six, three and one respectively in the first, second and third stage. Liquid oxygen and paraffin-based fuel are considered as propellants combination. A blow-down feed system is assumed to ensure system simplicity and reduce the overall launcher cost. An airborne launch is proposed at given altitude and speed whereas the velocity angle on the horizon at first stage ignition is set free. The optimization procedure of the engine design parameters employs a direct method and an evolutionary algorithm in the deterministic and robust-based approach, respectively. An indirect method is used to optimize the ascent trajectory given the engine design in both the approaches. In the robust-based approach, uncertainties in the fuel regression rate are taken into account. Small-launcher initial mass is given and payload mass is maximized for a given insertion orbit. A mission specific objective function is used in the robust-based optimization process to grant the actual achievement of mission goals, despite the uncertainties in the design. Two different design strategies are compared. In the first case the acceleration at first stage ignition is fixed, while in the second case the initial thrust is optimized. Results show that a 5-ton hybrid-rocket launcher can be viable for launch of satellites in the 50-100 kg range and that a small payload reduction, with respect to deterministic optimized solutions, is sufficient to ensure mission accomplishment and also grant the required design robustness.

Nomenclature

A_b = burning surface area, m^2

A_p = port area, m^2

A_{th} = nozzle throat area, m^2

*Acknowledgement: presented at the AIAA Propulsion and Energy 2019 Forum, 19-22 August 2019, Indianapolis, IN, Paper AIAA 2019-4096.
†Professor, Department of Mechanical and Aerospace Engineering, Corso Duca degli Abruzzi, 24, AIAA Senior member.
‡Research Assistant, Department of Mechanical and Aerospace Engineering, Corso Duca degli Abruzzi, 24.
§Professor, Department of Mechanical and Aerospace Engineering, Corso Duca degli Abruzzi, 24, AIAA Associate fellow.

a = regression constant, $\mathrm{m}^{1+2n}\ \mathrm{kg}^{-n}\ \mathrm{s}^{n-1}$

$\boldsymbol{b}$ = design parameters vector

C_F = thrust coefficient

c^* = characteristic velocity, m/s

$\boldsymbol{D}$ = drag vector, N

D = rocket outer diameter, m

E = nozzle area-ratio

$\boldsymbol{F}$ = thrust vector, N

F = thrust, N

G = gravitational constant, $\mathrm{m}^3\mathrm{kg}^{-1}\mathrm{s}^{-2}$

$\boldsymbol{g}$ = gravity acceleration, $\mathrm{m/s}^2$

h = altitude, km

h^* = target altitude, km

J = throat area to initial port area ratio

k = merit function constant, kg/km

L = overall engine length, m

l_g = grain length, m

M = rocket mass, kg

$M_\oplus$ = Earth mass, kg

m = mass, kg

P = burning perimeter, m

p = pressure, bar

$\boldsymbol{p}$ = uncertain parameters vector

R = grain port radius, m

R_g = grain outer radius, m

R_{th} = throat radius, m

$\boldsymbol{r}$ = position vector, m

t = time, s

$\boldsymbol{v}$ = velocity vector, m/s

V_g = pressurizing gas volume, m^3

w = web thickness, m

Z = hydraulic resistance, 1/(kg m)

α = mixture ratio

γ = specific heat ratio

Δ_{avg} = average height violation

Δv = velocity gain, km/s

λ_x = adjoint variable to state variable x

μ = payload mass, kg

ρ = density, kg/m^3

Φ_{avg} = robust optimization merit function

Superscripts

$\dot{}$ = time derivative

Subscripts

0 = ambient

1 = first-stage burnout

2 = second-stage ignition

3 = second-stage burnout

4 = third-stage ignition

5 = start of coast arc

6 = end of coast arc

7 = third-stage burnout

c = chamber/nozzle stagnation

$c1$ = combustion chamber at head-end

C_F = thrust coefficient

c^* = characteristic velocity

d = dry

e = nozzle exit

F = fuel

f = final value

i = initial value

L = lower bound

O = oxidizer

p = overall propellant (oxidizer + fuel)

t = oxidizer propellant tank

tot = total

U = upper bound

vac = vacuum

I. Introduction

Since the first launched CubeSats put in orbit in 2003, small satellites become more and more attractive over time. At the beginning, they were mostly meant as academic/research projects, while nowadays the majority of small satellites launched are for non-academic purposes and a lot of specialized small and medium-sized enterprises are emerging in this field. The availability of relatively cheap miniaturized technologies and novel information tools allow for the realization of distributed small satellite constellations, and almost 70 constellation projects have been recently announced with telecommunication or earth observation purposes. Therefore, the demand in term of launches for satellites having 200 kg mass or less is growing fast, and a dramatic increase is expected in the next future. Despite some threats and uncertainty (e.g. ground-based systems or drones giving similar services, debris, and International Telecommunication Union regulations), small satellites are considered a sound business opportunity. According to a recent market analysis* "the small satellite market is projected to reach USD 7.53 Billion by 2022."

Until recently, operative launchers designed for low-weight payloads were an exception (e.g. Pegasus XL) and access to space of CubeSats and other small spacecraft are still mainly based on piggyback launch or cluster launch. Due to this reasons, a large number of projects have started all around the world to develop dedicated launch systems, in order to provide an adequate answer to small satellites market requests.[1] At the date, several small satellite launchers are reported to be operative: Electron of Rocket Lab (New Zealand),[2] Fei Tian 1 / Kuaizhou-1A of CASIC / ExPace (China), Zhuque-1 of LandSpace (China),[3] OS-M of One Space (China) and Jielong-1 of China Rocket (China). Moreover, around fifty new small satellite launchers, currently under development, are expected to be operative in the next 5 years. Some examples are: LauncherOne of Virgin Galactic,[4] Alpha of Firefly[5] and Arion 2 of PDL Space.[6] The rise in the number of project concerning small satellite launchers is related to the intriguing commercial role that this kind of launch vehicle could assume in the near future.†

Due to their features,[7] Hybrid Rocket Engines (HRE) are promising propulsion systems for small sat launcher. Their performance is similar to that of storable or semi-cryo liquid rocket engines and they share appealing features of both solid rocket motors and liquid rocket engines. Moreover, they are cheaper and safer than liquid and solid rockets, and, in many cases, they are more environmentally friendly than storable liquid and solid rockets. Despite the aforementioned appealing features, they also present some drawbacks, such as low solid fuel regression rate[8] and the coupling between the mixture-ratio value and the thrust level. These drawbacks, in conjunction with the

*https://www.marketsandmarkets.com/Market-Reports/small-satellite-market-150947396.html

†Niederstrasser, Carlos and Frick, Warren. Small Launch Vehicles-a 2018 State of the Industry Survey. 2018.

lack of substantial funding, hindered HRE development as compared to solid and liquid counterparts. More recently, interest has grown to develop HRE for specific applications such as small-sat launcher. In 2018 Nammo launched a HRE sounding rocket above 100 km, an important step towards the development of a small-sat launcher.[9] Two small-sat launcher systems have been recently supported by the European Union's Horizon 2020 research and innovation programme, both include the development of hybrid rocket engines to power the launcher. One launcher system called ALTAIR ("Air Launch space Transportation using an Automated aircraft and an Innovative Rocket"),[10] considers an air-launched system powered by hybrid rockets. In the other program, called SMILE ("SMall Innovative Launcher for Europe"),[11, 12] a ground launch is considered. Both hybrid rocket engines and liquid rocket engines are considered and compared. In 2020, the European startup HyImpulse, founded as a spinoff of the Deutsches Zentrum für Luft- und Raumfahrt (DLR), has crowned its effort in the development of hybrid propulsion successfully testing a 75kN engine.[13] Such HRE will be used in sounding rockets and in a three stage small-sat launcher whose maiden launch is currently planned for 2022.

Budget and time required for the development of HREs can be reduced if a proper conceptual design is carried out. Multidisciplinary design optimization can be used to improve performance. The propulsion needs are strictly related to the mission to be carried out and a coupled optimization of the propulsion system and trajectory is required. This is especially true for HREs, which are one-lever control engines and usually exhibit varying thrust profile and mixture ratio shifting. The authors have developed proper tools to perform optimization of HRE for different applications,[14, 15] including an upper stage for a Vega-like launcher (1500-2000 kg payload),[16] and airborne launch for suborbital missions.[17]

However, in these previous works, optimization has been carried out from a deterministic point of view: no uncertainties in mathematical model parameters have been taken into account. Even small uncertainties in critical aspects, such as fuel regression rate determination, showed a catastrophic impact on HRE performance leading to mission failures.[18] Thus a robust-based approach has been developed and applied to the optimization of upper stages.[19–21] Results showed that robustness in the design (i.e. the fulfillment of mission requirements, despite the presence of uncertainties[22, 23]) is achieved at the cost of a small payload reduction.

In the present work the optimization of a HRE-powered 5000-kg launcher is carried out. The hybrid engines considered in the present analysis use liquid oxygen (LOX) and paraffin-based solid fuel as propellant combination and have a blow-down feed system. The choice of these specific propellants and feed system derives from a preliminary qualitative down-selection whose criteria include low cost, safety, reliability, simplicity, and environmental friendliness, as outlined below. Different choices may also lead to viable designs, but a full quantitative comparison is of out of the scope of the present work. The chosen propellant combination presents a good specific impulse and a large regression rate, and has shown promising performance when applied to sounding rockets and upper stages.[16, 24] The high performance is due to LOX, which is also relatively safe, environmentally friendly, low cost and is widely used in the

space launch industry.[25] On the other hand LOX is cryogenic and it requires low values of mixture ratio to give high specific impulse when burning with fuels containing hydrocarbons. The latter characteristic is a drawback when low fuel regression rates occur: this issue is solved using paraffin-based fuels. In fact, paraffin-based fuels[26] allow for good regression rate when compared to more classical solid fuels such as Hydroxyl-terminated Polybutadiene and High Density Polyethylene. This feature allows for the use of simple single hole fuel grains and suitable engine geometries to obtain the desired thrust levels while keeping the required low mixture-ratio values. As far as storability is concerned, most common storable oxidizers include highly concentrated Hydrogen Peroxide (HP), Nitrogen TetrOxide (NTO), nitric acid and its variants, and nitrous oxide. Nitric acid and NTO present physical hazards and environmental concerns. Nitrous oxide can be suitable for a low Δv missions such as suborbital flight but has too low performance for a launcher. A promising alternative to LOX could be HP, used in concentrated form up to 99%. Despite being unstable under certain conditions, HP can be storable with proper stabilizers. On the other hand, the use of HP determines lower characteristic velocity than LOX and requires a catalytic bed, possibly increasing masses and costs. Therefore, LOX is preferred for the present analysis.

The simplest blow down gas pressure feed system is here selected. Launcher performance can be improved by using a regulated gas pressure feed system. Nevertheless, nor a regulator neither a separated pressurizing-gas vessel is required with the selected blow down system, thus lowering complexity and costs. An electrically driven turbo pump may be an attractive choice for a high-performance launcher, but development costs and reliability may be a concern. The propellant combination adopted here guarantees sufficiently good performance even when simplicity and reliability are preferred for the feed system, in spite of the performance decay.

The optimization of the small-satellite launcher is here performed both from a deterministic point of view and employing a robust-based optimization approach. A reference orbit and an airborne launch condition are selected. Two different design approaches are considered and compared. In the following, Section III presents the launcher architecture and the engine modeling according to the deterministic approach and to the robust-based one, Section IV presents the trajectory optimization. In the end, results for the optimized solutions are reported and compared.

II. Launcher Architecture and Engine Model

The rocket has three stages, in analogy to the ALTAIR, SMILE and HyImpulse launch system concepts. Each stage employs the same hybrid engine in different numbers. Six engines are used in the first stage, three in the second stage, and one in the third stage. The number of engines in each stage is selected in order to have an almost uniform split of the Δv, similar acceleration levels and mass fractions between the stages. Most small launcher show payload fractions μ/m_i between 0.01 and 0.02. Thus, the initial mass is fixed at 5000 kg for a target design payload in the range from 50 kg to 100 kg. Interstage 1-2 adapter mass is 50 kg, interstage 2-3 adapter plus fairing (released at stage 2 jettisoning) sum up to 35 kg. These values are estimated as fractions of stages and engines masses in the early design phase. Coast arcs of 8

s are allowed for stage jettisoning in analogy to other existing launchers.[27]

The performance of the chosen propellant combination is evaluated [28] as a function of the mixture ratio α, assuming a chamber pressure $p_c = 10\,\text{bar}$. Even though the actual pressure in the combustion chamber can span over a wide range during engine operations, the error is small for the ranges of chamber pressure and mixture ratio experienced for the case here considered. An isentropic expansion with no change in gas composition is assumed to occur throughout the nozzle (ideal frozen equilibrium) to evaluate c^*, which is then corrected by a constant 0.96 factor.[25] Third-degree polynomial curves approximate the characteristic velocity and specific heat ratio to compute the proper values as the mixture ratio changes during engine operations. The thrust coefficient is evaluated as a function of nozzle area expansion ratio and ambient pressure is defined; constant specific heat ratio and isentropic expansion are given and a 0.98 C_F-efficiency is introduced to take losses into account:[25]

$$C_F = 0.98 \left\{ \sqrt{\frac{2\gamma^2}{\gamma-1}\left(\frac{2}{\gamma+1}\right)^{\frac{\gamma+1}{\gamma-1}}\left[1-\left(\frac{p_e}{p_c}\right)^{\frac{\gamma-1}{\gamma}}\right]} + E\frac{p_e}{p_c} \right\} - E\frac{p_0}{p_c} \tag{1}$$

A cylindrical grain with a single circular port is considered and uniform regression rate along the port axis is assumed.

$$\frac{\mathrm{d}R}{\mathrm{d}t} = a\left(\frac{\dot{m}_O}{A_p}\right)^n \propto \dot{m}_O^n \; R^{-2n} \tag{2}$$

with $a = 9.1 \cdot 10^{-5}\ \mathrm{m^{2n+1}s^{n-1}kg^{-n}}$ and $n = 0.69$, in nominal operating conditions.[26]

The contribution to the combustion process of the lateral ends of the fuel grain is here neglected. The chamber head-end pressure p_{c1} depends on the chamber/nozzle stagnation pressure p_c according to an approximate relation similar to that proposed by Barrere et al. for side-burning grains:[29]

$$p_{c1} = \left[1 + 0.2\left(\frac{A_{th}}{A_p}\right)^2\right] p_c \tag{3}$$

The hydraulic resistance Z in the oxidizer flow path from the tank to the combustion chamber, which is assumed to be constant during engine operation, determines the oxidizer flow rate. Under the assumption of incompressible turbulent flow:

$$\dot{m}_O = \sqrt{(p_t - p_{c1})/Z} \tag{4}$$

The fuel mass flow and the propellant mixture ratio are given by:

$$\dot{m}_F = \rho_F A_b \frac{\mathrm{d}R}{\mathrm{d}t} \propto \dot{m}_O^n \; R^{1-2n} \tag{5}$$

$$\alpha = \frac{\dot{m}_O}{\dot{m}_F} \propto \dot{m}_O^{1-n} \; R^{2n-1} \tag{6}$$

Concerning chamber pressure, one has:

$$p_c = \frac{(\dot{m}_O + \dot{m}_F)c^*}{A_{th}} \tag{7}$$

As stated in SectionI, a simple blow down pressurization system is adopted. In multi-engine stages (i.e. first and second stage), each hybrid engine is fed by its own oxidizer tank, in order to ease the production of the engines and, at the same time, have greater flexibility of launcher performance. According to the chosen ballistic model, the design of the HRE is defined by initial thrust F_i, initial mixture ratio α_i, nozzle expansion ratio E, initial value of tank pressure $(p_t)_i$, and initial gas volume in the oxidizer tank (ullage volume) $(V_g)_i$. The initial value of the chamber pressure is fixed at $(p_c)_i = 0.4\,(p_t)_i$. In general, the ratio p_t/p_c varies during operation, but the proposed value is usually sufficient to grant $p_t/p_c > 2.5$ for the whole burn duration. This margin is usually sufficient to avoid coupling between the hybrid engine and the oxidizer feed system. The initial port area to throat area ratio J should be as large as possible but is fixed at 0.5 to avoid excessive pressure losses and nonuniform grain regression. Preliminary calculations showed that the optimal tank pressure tends to be very low when it is left free. In order to avoid too low values of the fuel grain regression rate, tank pressure value is here fixed at 25 bar and is dropped from the set of optimization variables.

Given the set of design parameters, the engine initial geometry is first determined. From α_i one obtains the initial values of c^* and γ; p_e/p_c can also be computed from E. The thrust coefficient C_F and $c = c^*C_F$ can then be evaluated, provided the ambient pressure, which is known. The initial thrust F_i gives the mass flow rates at ignition

$$(\dot{m}_p)_i = (1 + \alpha_i)(\dot{m}_F)_i = \frac{1 + \alpha_i}{\alpha_i}(\dot{m}_O)_i = \frac{F_i}{c_i^*(C_F)_i} \tag{8}$$

The throat area A_{th} is determined from Eq. (7) and throat erosion is neglected in this analysis. Means to take its effect into account are however available.[16, 24]. The initial port area and radius are obtained as $(A_p)_i = \pi R_i^2 = A_{th}/J$. Also, the initial burning area is determined from Eq. (5), and the grain length $l_g = (A_b)_i/(2\pi R_i)$ is obtained, thus defining the initial grain geometry.

The tank pressure p_t rules engine operation and during blow down it is calculated assuming an isentropic expansion of the pressurizing gas in the tank,

$$p_t = (p_t)_i \left[\frac{(V_g)_i}{V_g}\right]^{\gamma_g} \tag{9}$$

where V_g is the gas volume in the propellant tank as a function of the generic oxidizer mass exhausted m_O at time t:

$$V_g = (V_g)_i + \frac{m_O}{\rho_O} \tag{10}$$

A. Deterministic Approach

Equations (2)-(7) are numerically solved to evaluate the regression rate, the propellants masses and flow rates during operation (and their ratio α), p_t, p_c and p_1, while the curve fit for c^* as a function of α is used. Then, the thrust level $F = p_c A_{th} C_F$ is determined, by evaluating C_F at the actual altitude, in order to integrate the trajectory equations. At burnout, the web thickness w and the grain outer radius $R_f = R_i + w$ are obtained; the overall propellant mass and an estimation of the structural masses are introduced to compute the engine overall mass.

The dry mass of the propulsion system is made of combustion chamber, nozzle, tanks and rocket casing; these are estimated by means of the following suitable assumptions and approximations. The combustion chamber has a 6-mm insulating liner (with density equal to that of the solid fuel) and an aluminum alloy cylindrical wall. The diameter of the aluminum cylindrical oxidizer tank is selected in order to have a given overall length-to-diameter ratio. The wall thicknesses of oxidizer tank and combustion chamber are determined to withstand internal pressure, assuming a 1.25 safety factor. Oxidizer tank valves and plumbing masses are accounted for in the adapter mass. Each HRE is encapsulated by a 1-mm thick cylindrical aluminum casing. A 45-deg convergent and a 20-deg divergent nozzle (half-opening angle) with a phenolic silica ablative layer is considered. A uniform thickness is assumed and evaluated to estimate the nozzle weight. The adopted thickness is half the value obtained according to Ref. [30] for the throat thickness; average values of the transport properties and an estimation of the heat flux at ignition are used. The nozzle structural mass is small compared to this ablative layer mass, which is obtained under conservative assumptions, and is thus neglected.

Two strategies will be discussed for the deterministic approach: in design A the initial thrust is fixed to have a proper initial acceleration (e.g., 1.4 g), whereas in design B the initial thrust is optimized. The engine design parameters are α_i and $(V_g)_i$ for design A and F_i, α_i and $(V_g)_i$ for design B. In both cases, nozzle expansion ratio E and aspect ratio L/D are fixed. In design A, E is selected to avoid flow separation in the nozzle; in design B to match nozzle and tank diameter. The aspect ratio is 10 for design A and is reduced to 7 for design B due to the larger structural loads. The engine design parameters are optimized with a direct method.[31] Tentative values are initially assumed for the free design parameters and the ascent trajectory is optimized by means of an indirect procedure to evaluate the payload.[32] Perturbation of the design parameter allow one to numerically evaluate the derivatives of the performance index and a procedure based on Newton's method is used to determine the set of design parameters which simultaneously nullify the index partial derivatives. Only a few minutes are sufficient to obtain the optimal design and the corresponding trajectory.

B. Robust Approach

In the robust approach two additional parameters are required to overcome combustion rate uncertainties: the first is the grain outer radius R_g, which makes it possible to determine the eventual fuel surplus, and the other one is the total oxidizer mass boarded $m_{O,tot}$, which gives the eventual oxidizer surplus. In contrast to the deterministic case, in

the robust solutions the nozzle expansion ratio is always optimized. Thus in the robust approach A, the optimization parameters result to be five: initial mixture ratio α_i, grain outer radius R_g, initial gas volume in the oxidizer tank (ullage volume) $(V_g)_i$, total oxidizer mass boarded $m_{O,tot}$ and nozzle expansion ratio E. In robust design B also the initial thrust F_i is optimized (in analogy with the deterministic B case). Optimization setups are summarized for the reader in Tab.1.

Table 1 Design parameters for the different optimization cases: number = parameter constrained at the given value, Opt. = optimization variable, NA = not required for the deterministic case.

Parameter	DET_A	DET_B	ROB_A	ROB_B
$(V_g)_i$	Opt.	Opt.	Opt.	Opt.
α_i	Opt.	Opt.	Opt.	Opt.
F_i	11.5 kN	Opt.	11.5 kN	Opt.
E	14	12.5	Opt.	Opt.
L/D	10	7	10	7
$m_{O,tot}$	NA	NA	Opt.	Opt.
R_g	NA	NA	Opt.	Opt.

Overall propellants and structural masses can be estimated, to compute the engine dry mass, once engine design is given fixing the design parameters, i.e. before trajectory optimization takes place. HRE dry mass is made of combustion chamber, nozzle, tanks and rocket casing masses, which are calculated as previously described for the deterministic approach. Payload mass μ is then calculated by subtracting the overall propellants masses and engine dry mass from the given launcher initial total mass (i.e. 5000 kg).

HRE operating condition is calculated by means of a numeric procedure as previously described in the Subsection A. In the robust-based approach, the web thickness w, the actual fuel mass burned and oxidizer mass exhausted at engine burnout are obtained during trajectory integration.

Engine design parameters are optimized by means of a particles swarm optimization (PSO) algorithm. Details about PSO can be found in Ref.[33]. Algorithm settings are summarized in Tab.2.

Table 2 PSO settings.

Number of generations, N_G	200
Number of particles, N_I	20
Dimension of particles	5
PSO method	1-trelea type 1
Cognitive acceleration, $C1$	2.0
Social acceleration, $C2$	2.0
Check population method	Saturation
End velocity weight	0.4
Linear varying factor	0.2
Mass mutation parameter	98%

Once engine and payload masses are computed, the ascent trajectory is optimized by means of an indirect procedure.[32] The target orbit is specified by means of altitude (800 km), eccentricity (zero) and inclination (95-deg, launch from 45 degree latitude). Only a few tens of seconds are sufficient to obtain the optimized trajectory, corresponding to the given set of design parameters. Nevertheless, the whole robust-based optimization requires approximately 300 hours on a single core 3 GHz machine, due to the high number of design points considered to properly manage the uncertainty in the design.

In the literature[23] the robust optimization problem is formally casted as:

$$\begin{aligned} &\text{find} && \boldsymbol{b} \in \mathbb{R}^n \\ &\text{to maximize} && \Phi_{avg}\left(\boldsymbol{b}, \boldsymbol{p}\right) \\ &\text{subject to} && g_j\left(\boldsymbol{b}, \boldsymbol{p} + z^p\right) \leqslant 0, j = 1, ..., r \\ &\text{and to} && \boldsymbol{b}_L \leqslant \boldsymbol{b} \leqslant \boldsymbol{b}_U \end{aligned} \tag{11}$$

where $\boldsymbol{p}$ is the uncertain parameters vector, z^p indicates the noise vector of $\boldsymbol{p}$, g_j is the j-th inequality constraint, $\boldsymbol{b}$ is the design parameters vector, $\boldsymbol{b}_L$ and $\boldsymbol{b}_U$ are the lower and upper boundary of the design parameters, respectively. In the present work design and uncertain parameters vectors are:

$$\boldsymbol{b} = [\alpha_i, R_g, (V_g)_i, m_{O,tot}, E] \tag{12}$$

$$\boldsymbol{p} = [a, n] \tag{13}$$

Uncertainties are taken into account by the authors assigning three different levels for each uncertain variables: $a_i \cdot 10^5 = 9, 9.1, 9.2\,\mathrm{m^{2n+1}s^{n-1}kg^{-n}}$ for $i = 1, 2, 3$, respectively, and $n_j = 0.68, 0.69, 0.7$ for $j = 1, 2, 3$, respectively.

Attained orbit altitude h_{ij} is evaluated for each of the nine possible couples a_i, n_j. An ϵ-constraint approach is adopted because two objectives are relevant (i.e. payload and altitude).[34] Only average performance is considered here. The average constraint violation is computed as $\Delta_{avg} = \sum_{ij} p_i p_j \max_{ij}(0, h^* - h_{ij})$. A binomial distribution is assumed, thus $p_1 = p_3 = 0.25$ and $p_2 = 0.5$. The average altitude $h_{avg} = h^* - \Delta_{avg}$ is then calculated and the problem merit function can be computed as:

$$\Phi_{avg} = \mu - k \max(0, \epsilon - h_{avg}) \tag{14}$$

The average altitude is forced to ϵ selecting $k = 20\,\mathrm{kg/km}$. In the present work the authors consider only the most demanding case (in terms of robustness) $\epsilon = h^* = 800\,\mathrm{km}$.

In this context, a further difference between deterministic and robust approach arise. In the deterministic approach the amount of oxidizer and fuel boarded are such that they end at the same moment at burnout and their masses are

optimized (i.e. minimized) to reach exactly the target orbit. On the other hand, in the robust optimization, the actual value of regression rate varies due to uncertainty. An higher than nominal regression rate means that all the fuel burns whereas there is still some unburned oxidizer, and on the contrary, a lower than nominal regression rate results in a condition such that all the oxidizer is exhausted whereas there is still some unburned fuel. In the end, a nominal regression rate means that fuel and oxidizer end at the same time.

The surplus in propellant mass required to reach (at least) target orbit, even in the higher/lower than nominal operation, result in a payload penalty for the robust design with respect to deterministic ones. Obviously, the robust designs are able to reach higher than target orbit when nominal regression rate occurs. However, in this context no altitude / velocity sensors are considered for engine shut down at target orbit. The authors assume that, if the launcher is able to reach at least the target orbit for every uncertain parameters combination, it is also able to reach exactly that orbit for every uncertain parameters combination.

III. Trajectory Optimization

Airborne launch is considered with starting conditions similar to the Pegasus launcher.[27] Rocket ignition occurs at 12 km-altitude, 45-deg latitude and 250 m/s speed, following a pull-up maneuver which is not modeled in this analysis. Payload is delivered to a reference circular orbit with 95-deg inclination. It is assumed that the initial velocity direction is free. The free molecular heat flux must remain below 1.136 $\mathrm{kW/m^2}$ (i.e., the conventional value of 0.1 $\mathrm{BTU/ft^2/s}$) after fairing jettisoning (second stage burnout). This is obtained by forcing a steep ascent trajectory with the introduction of a height constraint at the end of the third-stage first burn (either 160 km or 185 km as discussed later). It is worth noting that this constraint has a small effect on performance: payload variation are below 1 kg when the altitude has a 10 km change in the deterministic approach.

During the first-stage burn the vehicle follows a zero-lift gravity-turn trajectory with thrust parallel to the relative velocity. Thrust direction is left free and optimized for the second and third stage. The third stage performs two burns; the second one is very short for orbit circularization and could eventually be performed by a payload engine, if present. The ascent trajectory is therefore modeled with the following phases: 1) zero-lift gravity-turn first stage burn; 2) 8-second coast arc for stage jettisoning; 3) second stage burn with optimal thrust direction; 4) 8-second coast arc for stage and fairing jettisoning; 5) third-stage first burn with optimal thrust direction; 6) coast arc (free length); 7) third-stage second burn with optimal thrust direction for circularization. The j-th phase starts at time t_{j-1} and ends at t_j. The final mass is maximized in the deterministic approach whereas, in the robust-based approach, the indirect procedure maximizes the final insertion altitude for each uncertain parameters combination given the engine design. A point-mass rocket is considered and the state equations in an inertial Earth-centered reference frame are:

$$\frac{\mathrm{d}\boldsymbol{r}}{\mathrm{d}t} = \boldsymbol{v} \qquad \frac{\mathrm{d}\boldsymbol{v}}{\mathrm{d}t} = -GM_{\oplus}\frac{||\boldsymbol{r}^3||}{\boldsymbol{r}} + \frac{\boldsymbol{F}-\boldsymbol{D}}{m} \qquad \frac{\mathrm{d}m}{\mathrm{d}t} = -\frac{F}{c} \tag{15}$$

where an inverse-square gravity field has been assumed and $D = (1/2)\rho_{atm} C_D S\, v_{rel}^2$ is the aerodynamic drag. The reference area is the sum of cross sections of the HRE used in each stage, and is thus determined by the HRE design. The relative velocity is $\boldsymbol{v}_{rel} = \boldsymbol{v} - \boldsymbol{\omega} \times \boldsymbol{r}$ where $\boldsymbol{\omega}$ is Earth's angular velocity. The drag coefficient C_D is assumed to vary with the Mach number according to a typical law for rockets (see figure 1), to take the most relevant effects of its influence into account; the same law is used for the three stages. The state equations have been implemented in non-dimensional form in the code in order to improve its convergence properties. The thrust is written as a function of the vacuum thrust $F = F_{vac} - E A_{th} p_{atm}$, where F_{vac} is a given function of time once the engine design has been specified. Numerical fits of Earth's atmosphere are used to determine pressure and temperature as functions of the altitude h, according to a simplified model.

Boundary conditions fix the initial (at $t_0 = 0$) position, relative velocity magnitude and mass. At final time t_f, insertion into a circular orbit with specified inclination is imposed (radius, vertical velocity, horizontal velocity magnitude and inclination are fixed) in the deterministic approach. On the other hand, in the robust-based approach the final altitude is free and maximized, whereas a specific constraint on burned fuel and oxidizer is imposed to avoid unfeasible solutions (i.e exhausted propellants masses higher than boarded ones). Since the same engines are used in each stage, the burning times must be the same. Therefore, the additional conditions $t_1 = t_3 - t_2 = t_7 - t_6 + t_5 - t_4$ are introduced. Also, the coast arcs $t_2 - t_1 = t_4 - t_3$ are given. As already stated, the height at t_5 is fixed in the deterministic approach.

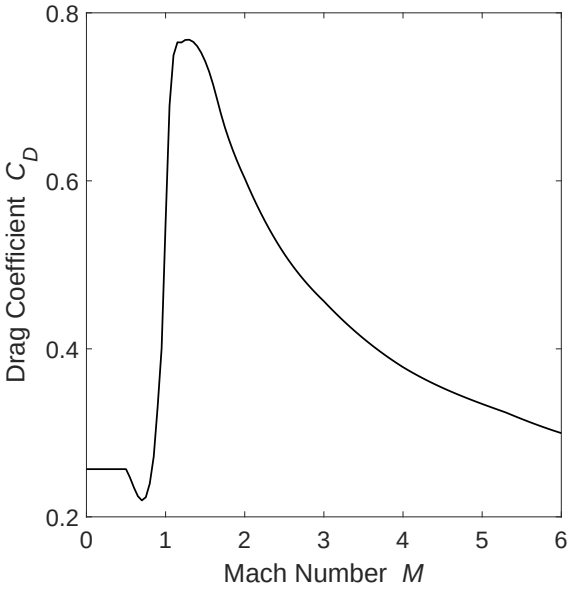

Fig. 1 Drag coefficient.

The theory of optimal control is applied to optimize the trajectory, once the characteristics of the stages are assigned. Adjoint variables are associated to the state equations and the Hamiltonian, which has different expressions depending on the phase of flight, is defined

$$H = \boldsymbol{\lambda}_r \boldsymbol{v} + \boldsymbol{\lambda}_v \left(\frac{\boldsymbol{r}}{|\boldsymbol{r}|^3} + \frac{\boldsymbol{F} - \boldsymbol{D}}{m} \right) - \lambda_m \frac{F}{c} \tag{16}$$

Optimal control theory provides the Euler-Lagrange equations for the adjoint variables

$$\frac{\mathrm{d}\boldsymbol{\lambda}_r}{\mathrm{d}t} = -\frac{\mathrm{d}H}{\mathrm{d}\boldsymbol{r}} \qquad \frac{\mathrm{d}\boldsymbol{\lambda}_v}{\mathrm{d}t} = -\frac{\mathrm{d}H}{\mathrm{d}\boldsymbol{v}} \qquad \frac{\mathrm{d}\lambda_m}{\mathrm{d}t} = -\frac{\mathrm{d}H}{\mathrm{d}m} \tag{17}$$

The optimal control theory (OCT) provides the thrust direction, when it is left free, which results to be parallel to

Table 3 Performance and design summary: deterministic optimization (800 km altitude).

Design	F_i	$(V_g)_i$	α_i	w	R_f	R_{th}	D	E	$m_{O,tot}$	m_F	m_d	μ
	kN	m^3	-	m	m	m	m	-	kg	kg	kg	kg
A	11.5	0.253	1.86	0.140	0.211	0.050	0.481	14	291.5	134.2	61.0	48.0
B	27.2	0.108	2.58	0.105	0.213	0.076	0.549	12.5	297.2	129.1	57.8	73.6

the velocity adjoint vector, also named the primer vector. OCT also provides boundary conditions for optimality at the initial and final point and at the boundaries of each phase.[32] The dual problem of radius maximization for given HRE mass (that is, payload) is preferred as it allows for an easier derivation of the optimality conditions. One obtains that the velocity adjoint vector must be parallel to the relative velocity vector at $t = 0$ and two additional conditions at the final time (here omitted), which relate values of position and velocity to their adjoint variables. In addition, OCT provides the transversality conditions to determine the relevant times. Time is formally free in this formulation (the time boundary conditions become mass constraints) and the Hamiltonian must be continuous at time t_5 and t_6 and null at t_7. At t_5 the radius adjoint variable has a free discontinuity and is an additional optimization variable; also, $\lambda_{rf} = 1$ and it is conveniently replaced by $\lambda_{r0} = 1$, reducing the number of unknowns. The mass adjoint variable has free discontinuities at times from t_1 to t_4 to assure Hamiltonian continuity, but since λ_m does not appear in the equation for the other variables and boundary conditions at those points, these discontinuities can be ignored.

The multi-point boundary value problem, which arises from the application of the theory of optimal control, is solved by a procedure based on Newton's method.[35] Tentative values are initially chosen for the problem unknowns and progressively modified to fulfill the boundary conditions.

IV. Results

A. Deterministic Optimization Results

Two different acceleration-constraint specifications are considered. The first analysis (design A) assumes a fixed initial thrust, whose level is chosen in order to have an initial acceleration about 1.4 g, i.e., a usual value in conventional launchers. To this purpose, the vacuum initial thrust of the hybrid rockets is here fixed to be 11.5 kN each, determining an initial acceleration of 1.406 g. The nozzle expansion area ratio must also be constrained at 14, in order to avoid separation at the ignition of the first stage.[36] In this analysis, an overall length to diameter ratio $L/D = 10$ is used. Therefore, only two optimization variables (namely, gas volume in the oxidizer tank and initial mixture ratio) remain. Results of the direct optimization of the engine design parameters are summarized in Table 3.

The vehicle needs a sufficiently large acceleration for a suitably long time in order to keep a steep trajectory that moves the vehicle out of the lower layers of the atmosphere. Also, drag is remarkable during the first stage burn, therefore a large thrust is a premium. To this aim, a large volume of pressurizing gas is required to avoid an excessive

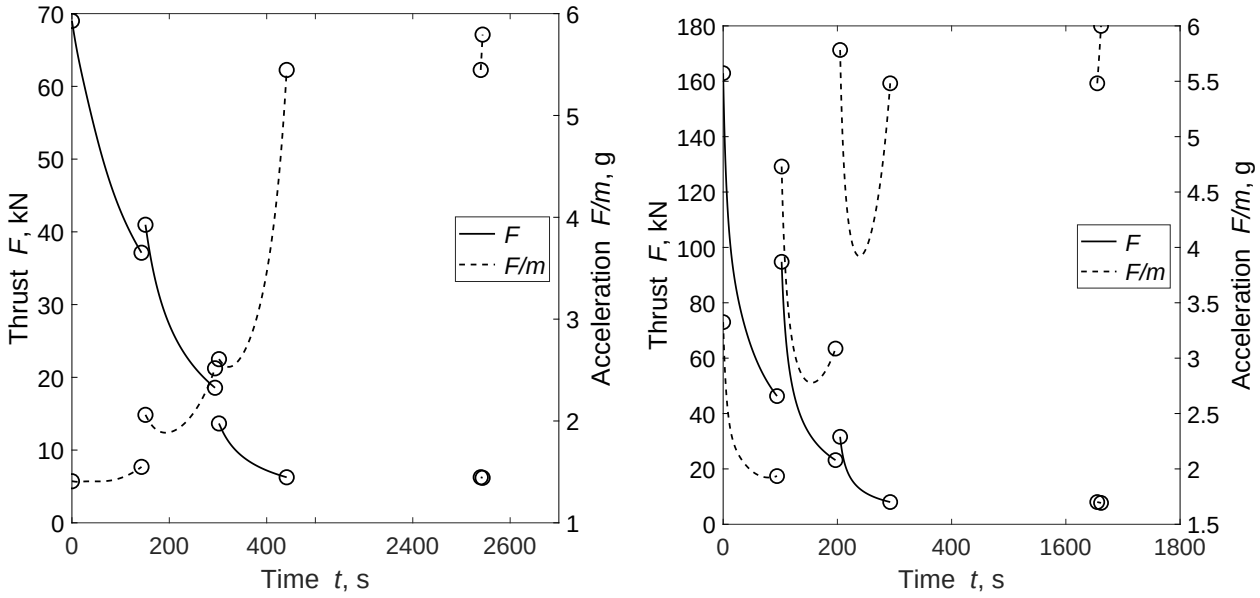

(a) Design A.

(b) Design B.

Fig. 2 Thrust and thrust acceleration history: deterministic optimization (800 km altitude).

drop in tank pressure and, consequently, of thrust magnitude. The selection of a low mixture ratio reduces the oxidizer flow and helps to alleviate this problem. Figure 2 shows the thrust and thrust acceleration histories. It is worth noting that the thrust magnitude is remarkably influenced by the altitude; for instance, one can observe that the initial thrust of the second stage is more than half the corresponding value of the first stage, despite using three engines versus six. The relatively small decrease of the thrust magnitude causes a constant increase of the acceleration, due to the strong mass reduction. Values at burnout of the final stage are relatively large and are close to 6 gs, which is a typical limit in launcher operation. Figure 3 shows the behavior of mixture ratio and specific impulse. The design optimization allows the mixture ratio to grow during engine operation; it increases towards the value corresponding to the optimal specific impulse (i.e., about 2.2), thus reducing the propellant consumption. The specific impulse at first stage ignition is greatly penalized by the over expanded operation. Larger values occur at the ignition of the other stages, due to the larger altitude. The height at burnout of the second stage is constrained to 160 km.

With the aim of improving performance, a different design (design B) is analysed, where the initial thrust is left free and optimized. In this case, however, the final value of acceleration must be constrained to avoid excessive loads, and 6 g is selected as upper limit. The results of the optimization procedure are compared to design A in Table 3. Design B presents larger initial thrust levels and, with the assumption that the initial pressure is the same as in Design A, the nozzle throat and exit area tend to become larger. A reduced values of length-to-diameter ratio (7) must be adopted and nozzle expansion area ratio is reduced (12.5) to approximately match engine outer diameter. Also, the height at burnout of the second stage must be increased to 185 km to avoid excessive heat flux. The strategy to optimize the payload is remarkably different from the previous case. With a large thrust available, greater drops in tank pressure and thrust

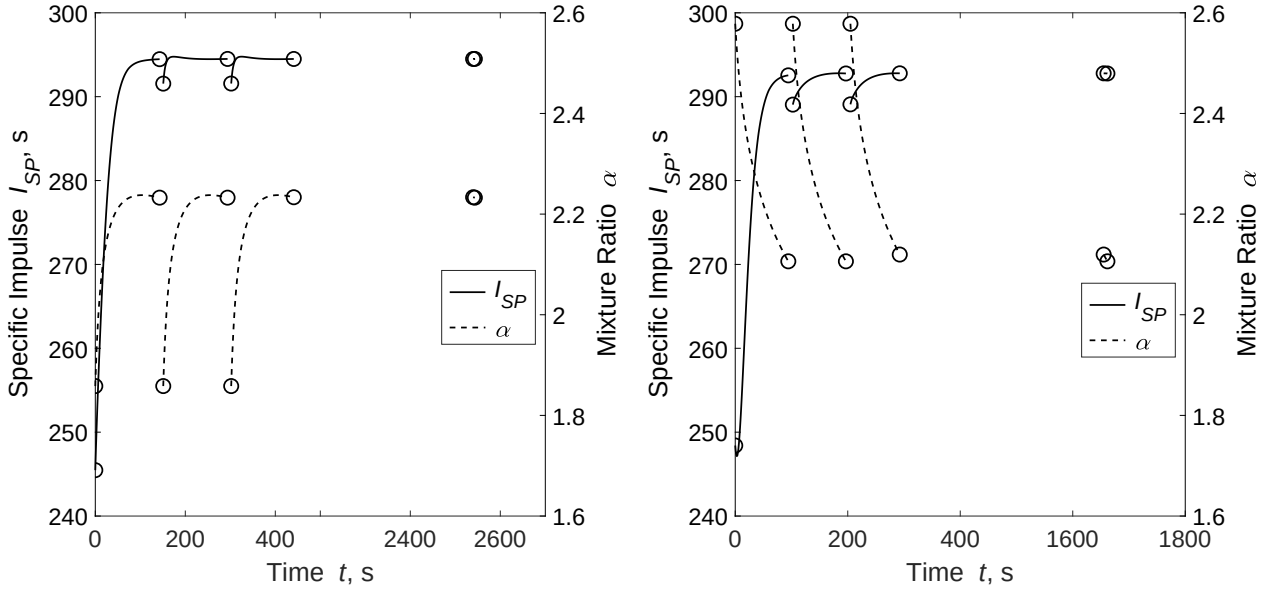

(a) Design A. (b) Design B.

Fig. 3 Specific impulse and mixture ratio history: deterministic optimization (800 km altitude).

can be accepted, and the pressurizing gas volume is greatly reduced. This allows for a smaller tank with a saving in terms of dry mass. The propellant load must be increased due to the lower specific impulse, associated to the lower nozzle expansion ratio, and the less efficient trajectory, which must become steeper to satisfy the thermal flux limitation. However, the trade off is beneficial, as 2.6 kg are saved in each hybrid motor, leading to a 25.6 kg increase of the payload.

The different philosophy of the two designs is highlighted by comparing in Fig. 2 thrust and thrust acceleration, and, in Fig. 3, specific impulse and mixture ratio. The lower pressurizing gas mass in Design B causes larger shifts in the engine performance and, overall, a higher average acceleration is experienced (i.e., the burning times are shorter). The peak acceleration is however quite similar. The mixture ratio tends to decrease during operation of Design B because of the larger drop in tank pressure which reduces the oxidizer flow rate. To maintain the average specific impulse at sufficient levels, a large value of initial mixture ratio must be selected. The altitude growth of the two designs is compared in Fig. 4. Design B has a faster increase both due to the larger thrust and the necessity of reaching a higher altitude at burnout of the second stage, to fulfill the heat flux constraint. Its shorter coast arc is related to the steeper trajectory.

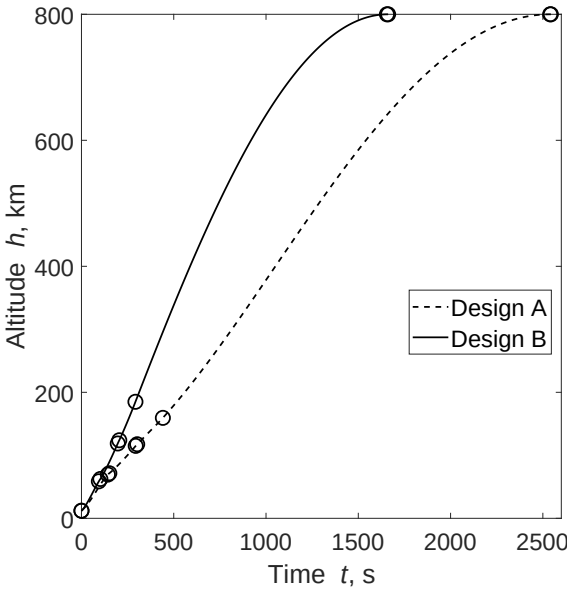

Fig. 4 Altitude growth comparison.

Table 4 Performance and design summary: deterministic optimization (700 km altitude).

Design	F_i	$(V_g)_i$	α_i	w	R_f	R_{th}	D	E	$m_{O,tot}$	m_F	m_d	μ
	kN	m^3	-	m	m	m	m	-	kg	kg	kg	kg
A	11.5	0.253	1.86	0.140	0.211	0.050	0.481	14	291.4	134.1	61.0	50.1
B	27.3	0.109	2.57	0.104	0.212	0.077	0.550	12.5	297.0	129.0	57.9	76.3

Table 5 Performance and design summary: deterministic optimization (800 km altitude).

Design	h_0	F_i	$(V_g)_i$	α_i	w	R_f	R_{th}	D	E	$m_{O,tot}$	m_F	m_d	μ
	km	kN	m^3	-	m	m	m	m	-	kg	kg	kg	kg
A	11	11.5	0.253	1.86	0.138	0.210	0.051	0.481	14	290.7	134.6	61.0	50.1
A	12	11.5	0.253	1.86	0.140	0.211	0.050	0.481	14	291.5	134.2	61.0	48.0
A	13	11.5	0.268	1.86	0.141	0.211	0.050	0.484	14	292.2	133.0	61.6	46.4
B	11	26.2	0.107	2.58	0.105	0.213	0.076	0.548	12.5	297.4	129.2	57.7	71.7
B	12	27.2	0.108	2.58	0.105	0.213	0.076	0.549	12.5	297.2	129.1	57.8	73.6
B	13	27.8	0.109	2.57	0.104	0.213	0.076	0.549	12.5	296.9	129.2	57.9	75.3

It is interesting to analyze the effect of orbit altitude on optimal design and corresponding performance; results for final altitude reduced from 800 to 700 km are shown in Table 4. Design A is substantially unchanged, and just a slightly smaller propellant mass is adopted, permitting an increase of payload of about 2 kg. On the other hand, design B prefers a slightly larger initial thrust in comparison to the 800 km case, with a small increase in dry mass. In this case, the propellant load is reduced (in particular, the oxidizer), and the payload gain is about 3 kg in both cases.

A final analysis has concerned the release altitude and Table 5 compares optimal design and performance for altitudes of 11, 12 (nominal) and 13 km. In agreement with intuition, the payload grows with the release altitude for design B, which is capable of selecting the most suitable initial thrust value. On the contrary, and counter-intuitively, the payload worsen when the release altitude is increased in design A. This fact is related to the constraint on the initial thrust. The same thrust at higher altitude implies a smaller vacuum thrust because a reduced ambient pressure must be faced. Therefore, the rocket released at 13 km experiences a lower average acceleration (the thrust growth with altitude is smaller) and flies a less efficient trajectory with larger gravitational losses. However, the optimization process changes the design and the mixture ratio to increase the specific impulse and reduce the propellant consumption. On the other hand, a larger pressurizing gas volume is required to maintain suitable mixture ratio values, and the increased dry mass offsets the propellant reduction. The additional freedom in selecting the initial thrust of design B avoids these complex interactions. Designs with similar vacuum thrust can be adopted at the different release altitudes. The payload growth is mainly related to the decreased propellant consumption, as the altitude gain that must be provided by the rocket is lower.

B. Robust Optimization Results

Robust optimization results for the design A (i.e. fixed initial acceleration/given initial thrust) are first presented. Upper and lower boundary of the design variables are shown in Tables 6. Figure 5 shows launcher performance during engine operation. In addition, Tab.7 compares robust design parameters values (ROB_A) and deterministic ones (DET_A) for 800-km altitude.

Table 6 Design parameters ranges for the robust design A.

	α_i	R_g	$(V_g)_i$	$m_{O,tot}$	E
	-	m	m^3	kg	-
$\boldsymbol{b}_L$	1.83	0.209	0.223	280	10
$\boldsymbol{b}_U$	1.88	0.213	0.283	300	14

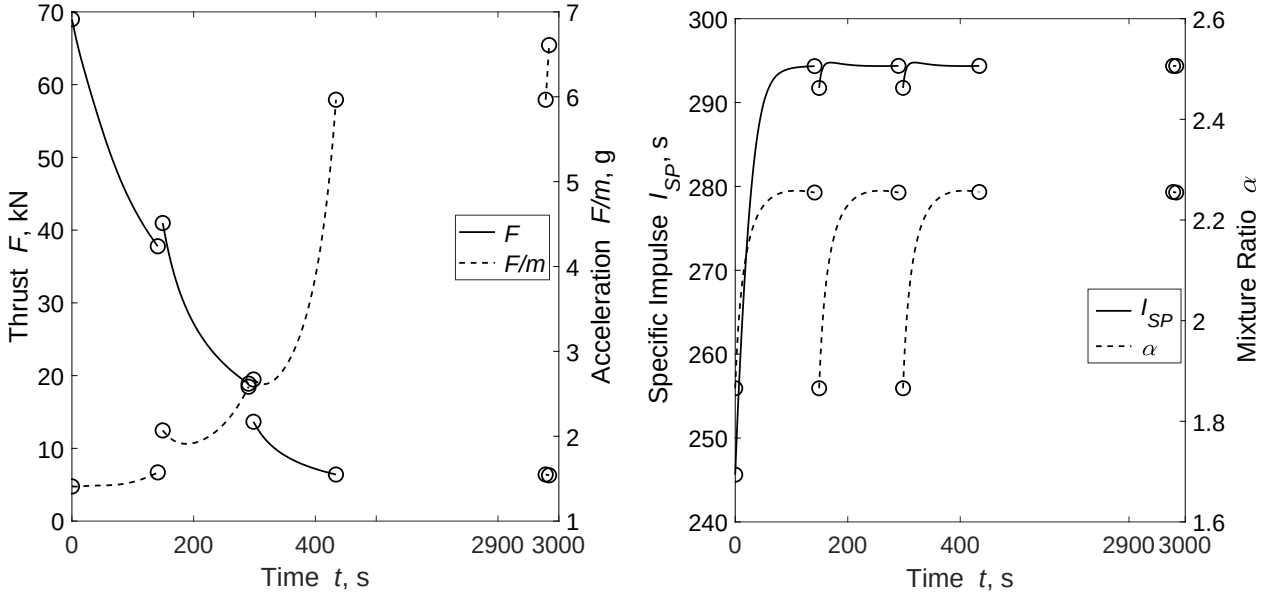

Fig. 5 Design A performance: robust optimization (800 km altitude).

ROB_A solution exhibits a slightly increased oxidizer mass and a decreased fuel mass with respect to DET_A values. This behavior is due to the selection of an higher initial value for the mixture ratio α_i when robustness is considered and to a different grain geometry. Fuel grain of the robust solution is actually shorter and has a slightly greater web thickness than deterministic one, resulting in a smaller throat area ($J = 0.5$ = constant), despite an almost equal grain outer radius R_g. One can notice that the robust solution exhibits a greater value of $(V_g)_i$ than deterministic one. This trend seems to be due to the need for a less decaying thrust level, during the engine burn, in order to mitigate uncertainties impact on performance (e.g. when regression rate is lower than nominal).

The nozzle expansion ratio was given and fixed to 14 in the deterministic optimization in order to avoid separation issues in the nozzle. On the other hand, in the robust optimization, E is a free design parameter. Nevertheless, the

optimal value of nozzle expansion ratio selected by the PSO is equal to 14 too: higher values of E result to be beneficial in terms of launcher payload, but the upper bound for E has to be fixed to the deterministic value of 14 (as reported in Tab.6) to avoid excessive over-expanded operation at first stage ignition for the robust optimized solution.

ROB_A engine dry mass is greater than DET_A one due to heavier casing and tank, reducing mass saving due to minor overall propellants mass. Thus, each HRE is roughly 1.3 kg heavier when robust design is adopted, resulting in a total payload reduction of approximately 14 kg, i.e. 28% of the deterministic payload.

Table 7 Performance and design comparison: deterministic design A (DET_A) vs. robust design A (ROB_A) (800 km altitude).

Design	α_i	R_g	$(V_g)_i$	$m_{O,tot}$	E	m_F	m_d	μ	Δ_{avg}	Φ_{avg}
	-	m	m^3	kg	-	kg	kg	kg	km	kg
DET_A	1.86	0.211	0.253	291.5	14.00	134.2	61.0	48.0	500.75	-9967.1
ROB_A	1.87	0.212	0.261	291.8	14.00	133.3	63.0	34.3	0.00	34.3

However, due to the large value of k used in Eq.(14), the ROB_A solution is capable of achieving the required altitude for any value of the uncertain parameters, whereas the DET_A solution shows an average height violation equal to more than 60% of the target altitude (i.e. 800 km): regression rate uncertainty leads to a rocket crash (i.e. $h_{ij} = 0$ km) for five out of nine test cases, when the DET_A solution is considered. The small launcher presents an altitude violation for the DET_A solution that is far greater than the one obtained for the upper stage optimized in Ref.[19]. The small launcher shows a consistent response to uncertainties in the design in terms of altitude violation, resulting in a large payload reduction when robust-based optimization is employed. This behavior is caused by the spread of performance degradation, due to uncertainties, from a stage to an other, requiring a very conservative solution.

Table 8 Design parameters ranges for the robust design B.

	α_i	R_g	$(V_g)_i$	$m_{O,tot}$	E
	-	m	m^3	kg	-
$\boldsymbol{b}_L$	2.30	0.210	0.100	290	9
$\boldsymbol{b}_U$	2.80	0.217	0.115	300	16

In order to improve launcher performance in terms of payload, a design B-like robust-based strategy is analyzed: the initial thrust is left free and optimized, whereas the final acceleration is constrained to 6 g, in nominal condition. Off-nominal conditions result in different initial thrust levels and different final accelerations. However, in off-nominal conditions, the final spacecraft mass is actually greater and the final acceleration smaller than in nominal condition due to the presence of fuel sliver (when regression rate is smaller than nominal) or unburned oxidizer (when regression rate is greater than nominal). Thus, the fulfillment of the imposed constraint on the final acceleration is granted for all uncertain parameters combinations. In addition, due to the design B-like nature of this analysis, an overall length to diameter ration L/D equal to 7 has been here considered by the authors. Upper and lower boundary of the design

variables in the design-B strategy are different from the ones previously presented in Table 6 and are shown in Table 8. The same settings for the PSO algorithm have been used in both the robust optimization procedures (see Tab.2).

Table 9 Performance and design comparison: deterministic design B (DET_B) vs. robust design B (ROB_B) and 5 g final acceleration design B (ROB_5) (800 km altitude).

Design	α_i	R_g	$(V_g)_i$	$m_{O,tot}$	E	m_F	m_d	μ	Δ_{avg}	Φ_{avg}
	-	m	m^3	kg	-	kg	kg	kg	km	kg
DET_B	2.58	0.213	0.108	284.4	12.50	134.0	57.8	73.6	321.17	-6349.9
ROB_B	2.60	0.214	0.103	297.2	12.39	130.1	57.3	68.3	131.15	-2554.6
ROB_5	2.53	0.216	0.097	296.2	15.53	131.0	58.5	58.3	50.31	-948.0

The results of the robust-based optimization for the design B are shown in Tab.9 and compared to the optimum solution of the deterministic design B. One can notice that the average altitude violation Δ_{avg} of the robust design is less than half the deterministic design one but still not passably close to zero, that is a necessary condition for the robustness in the design. For this reason, the value of the robust-based optimization merit function Φ_{avg} is negative for both deterministic and robust solution, albeit being far smaller in absolute value for the robust solution. The minimum insertion altitude for the robust-based design is equal to 339.4 km and is obtained when the regression rate assumes its highest value (i.e. both regression rate correlation coefficient and exponent equal to their greater than nominal values). Moreover, only three out of nine uncertain combinations lead to acceptable orbit altitudes ($\geq$ 800 km). Thus the optimized solution for the robust-based B-like strategy is not able to match the robustness requirements for the small launcher design.

In order to improve robustness in the solution the authors carried out two different strategies. First, larger ranges of variation $\boldsymbol{b_L}$ and $\boldsymbol{b_U}$ and longer optimization runs (N_G = 1000) have been adopted. Nevertheless, this strategy did not result in better performance, in terms of solution robustness; the obtained optimized solution for the robust design B seems to be the actual global optimal solution for the considered robust model and design strategy.

The second strategy considers that, in general, spacecraft final mass in the robust solutions results greater than the deterministic one, despite the smaller payload mass. As previously recalled in Section B, this fact depends on the propellant surplus required to withstand the uncertainty in the combustion process in off-nominal conditions. On the other hand, the constraint on the final acceleration fixes the final thrust level, given the engine design, penalizing the off-nominal performance of robust optimal solutions. Thus, in order to weaken this constraint, we lowered the value of the final acceleration of the spacecraft to 5 g. The results of this improving strategy are reported in Tab.9 as ROB_5. The minimum insertion altitude is equal to 519.4 km which is a 53% improvement with respect to the ROB_B solution, whereas launcher payload is reduced by 10 kg. The robustness in the design is greater, since the optimization merit function value has grown. However, the average altitude violation is still unacceptable for a truly robust optimal

solution, requiring all insertion altitude greater than or equal to the target mission altitude. Further reduction in the final acceleration constraint could improve solution robustness, but the resulting design will be far from the original B optimization strategy. The conclusion is that the Design B, despite better performance, can not lead to a proper robust solution.

V. Conclusions

A coupled direct-indirect deterministic optimization procedure is employed to design a hybrid-rocket launcher for small satellites (up to about 80 kg). The same engine is used in different numbers in the three stages to minimize development costs. An airborne-launched vehicle is considered. There is a complex performance dependence on the design parameters, but the optimization procedure allows for satisfactory design in the presence of different constraint (e.g., initial or final acceleration, heat flux, etc.). The design variables are adjusted by the optimization procedure to fulfill the imposed constraints, while maintaining adequate payload. Different designs with similar performance may be available; additional considerations (e.g., about cost) may drive the final selection. The developed optimization procedure appears to be fundamental to deal with the complex interactions between engine design and trajectory. The initial altitude has a peculiar effect on performance and engine design parameters and further studies should be performed to get a better comprehension of the interactions and possibly improve the payload for the same initial mass.

In the robust-based approach, a coupled evolutionary/indirect procedure is employed to optimize the design of the same hybrid-rocket launcher for small satellites. A mission specific merit function is used, in order to nullify the effects of uncertainties on mission goals, i.e. forcing the altitude violation to zero. The authors take into account the presence of uncertainties in the hybrid combustion process, which may lead to deviations of the regression rate from its nominal value and residual propellants, altering the actual HRE performance. Results show that the required robustness in the design is achievable but at the cost of a remarkable payload reduction with respect to the deterministic optimized solutions. An alternative design strategy (free initial thrust/constrained final acceleration), which determines the best performance in the deterministic approach, results unable to grant the adequate robustness in the design when employed in the robust-based procedure. A final remark should be added about the assumption that each HRE experiments the same off-nominal condition when uncertainties come into play. This assumption drastically reduces the computational cost, but could represent a possible limitation of the current work since the most demanding cases are faced simultaneously by each engine, strongly conditioning the resulting robust optimal design and the performance of the launcher. In future works, a different robust-based approach, able to treat the uncertainties of each engine individually, will be considered. Better launcher performance are expected, considering that the probability of every engine operating in the most unfavorable conditions is very low.

References

[1] Pelton, J. N., and Madry, S., *Handbook of Small Satellites; Technology, Design, Manufacture, Applications, Economics and Regulation*, 2020.

[2] Bailey, M., "Frequent and Reliable Launch for Small Satellites: Rocket Lab's Electron Launch Vehicle and Photon Spacecraft," *Handbook of Small Satellites: Technology, Design, Manufacture, Applications, Economics and Regulation*, 2020, pp. 1–17.

[3] Geng, H., LEI, Z., and YAWEI, X., "The Design, Implementation and Test Flight Result of the First Chinese Commercial Launch Vehicle System, ZQ-1," *2019 IAC*, 2019.

[4] Charania, A., Isakowitz, S., Matsumori, B., Pomerantz, W., Vaughn, M., Kubiak, H., and Caponio, D., "LauncherOne: Virgin Galactic's Dedicated Launch Vehicle for Small Satellites," 2016.

[5] Markusic, T., Sabripour, S., King, P., and Bradford, A., "Firefly–A New Generation of Low Cost, Small Satellite Launch Vehicles Designed to Serve the Rapidly Growing Small Satellite Market," *Proceedings of the 13th Reinventing Space Conference*, Springer, 2018, pp. 39–47. doi:https://doi.org/10.1007/978-3-319-32817-1_5.

[6] Torres, R., and García, F., "PLD Space'Arion 2 micro-launcher; simplifying and improving the responsiveness in launch operations." *2018 SpaceOps Conference*, 2018, p. 2467.

[7] Altman, D., and Holzman, A., "Overview and history of hybrid rocket propulsion," *Progress in Astronautics and Aeronautics*, Vol. 218, 2007, pp. 1–36.

[8] Pastrone, D., "Approaches to low fuel regression rate in hybrid rocket engines," *International Journal of Aerospace Engineering*, Vol. 2012, 2012. doi:https://doi.org/10.1155/2012/649753.

[9] Faenza, M., Boiron, A. J., Haemmerli, B., and Verberne, C. J., "The Nammo Nucleus Launch: Norwegian Hybrid Sounding Rocket over 100km," *AIAA Propulsion and Energy 2019 Forum*, 2019, p. 4049. doi:10.2514/6.2019-4049.

[10] Bérend, N., Gauvrit-Ledogar, J., Karl, C., Romano, D. G., Haemmerli, B., and AS, N. R., "ALTAIR Semi-Reusable Air-Launch System-Current Design and Status of Flight Experiments," 2019. doi:10.13009/EUCASS2019-830.

[11] Oving, B., Van Kleef, A., Haemmerli, B., Boiron, A., Kuhn, M., Müller, I., Petkov, I., Petrozzi, M., Neculaescu, A.-M., Afilipoae, T. P., et al., "Small Innovative Launcher for Europe: achievement of the H2020 project SMILE," *Proceedings of the 7th EUCASS conference, paper*, Vol. 600, 2017. doi:10.13009/EUCASS2017-600.

[12] Timmermans, L., Bernving, N., Van Kleef, A., Haemmerli, B., Kuhn, M., Muller, I., Petrozzi, M., and Psoni, G., "Small Innovative Launcher for Europe: Results of the H2020 Project SMILE," *2019 IAC*, 2019.

[13] Schmierer, C., Kobald, M., Fischer, U., Tomilin, K., Petrarolo, A., and Hertel, F., "Advancing Europe's Hybrid Rocket Engine Technology with Paraffin and LOX," *Proceedings of the 8th European Conference for Aeronautics and Space Sciences*, 2019. doi:10.13009/EUCASS2019-682.

[14] Casalino, L., and Pastrone, D., "Integrated Design-Trajectory Optimization for Hybrid Rocket Motors," *Modeling and Optimization in Space Engineering*, edited by G. Fasano and J. Pinter, Springer, New York Heidelberg Dordrecht London, 2013, pp. 343–362. doi:10.1007/978-1-4614-4469-5_14.

[15] Casalino, L., and Pastrone, D., "Optimal Design of Hybrid Rocket Motors for Launchers Upper Stages," *Journal of Propulsion and Power*, Vol. 26, No. 3, 2010, pp. 421–427. doi:10.2514/1.41856.

[16] Casalino, L., Letizia, F., and Pastrone, D., "Optimization of Hybrid Upper-Stage Motor with Coupled Evolutionary/Indirect Procedure," *Journal of Propulsion and Power*, Vol. 30, No. 5, 2014, pp. 1390–1398. doi:10.2514/1.B35111.

[17] Casalino, L., and Pastrone, D., "Optimal Design and Control of Hybrid Rockets for Access to Space," Paper AIAA 2005-3547, AIAA, 2005. doi:10.2514/6.2005-3547.

[18] Casalino, L., and Pastrone, D., "A Straightforward Approach for Robust Design of Hybrid Rocket Engine Upper Stage," *51st AIAA/SAE/ASEE Joint Propulsion Conference*, 2015, p. 4202. doi:10.2514/6.2015-4202.

[19] Casalino, L., Masseni, F., and Pastrone, D., "Robust Design Approaches for Hybrid Rocket Upper Stage," *Journal of Aerospace Engineering*, Vol. 32, No. 6, 2019. doi:10.1061/(ASCE)AS.1943-5525.0001078.

[20] Casalino, L., Masseni, F., and Pastrone, D., "Uncertainty Analysis and Robust Design for a Hybrid Rocket Upper Stage," *Journal of Spacecraft and Rockets*, 2019, pp. 1–8. doi:10.2514/1.A34422.

[21] Casalino, L., Masseni, F., and Pastrone, D., "Viability of an Electrically Driven Pump-Fed Hybrid Rocket for Small Launcher Upper Stages," *Aerospace*, Vol. 6, No. 3, 2019, p. 36. doi:10.3390/aerospace6030036.

[22] Taguchi, G., Chowdhury, S., and Taguchi, S., *Robust Engineering*, Vol. 224, McGraw-Hill New York, 2000.

[23] Park, G., Lee, T., Lee, K., and Hwang, K., "Robust Design: an Overview," *AIAA journal*, Vol. 44, No. 1, 2006, pp. 181–191. doi:10.2514/1.13639.

[24] Casalino, L., Letizia, F., and Pastrone, D., "Design Trade-offs for Hybrid Rocket Motors," Paper AIAA 2012-4202, AIAA, 2012. doi:10.2514/6.2012-4202.

[25] Sutton, G. P., and Biblarz, O., *Rocket Propulsion Elements*, 7^{th} ed., John Wiley & Sons, New York, NY, 2001.

[26] Karabeyoglu, M., Altman, D., and Cantwell, B., "Combustion of Liquefying Hybrid Propellants: Part 1, General Theory," *Journal of Propulsion and Power*, Vol. 18, No. 3, 2002, pp. 610–620. doi:10.2514/2.5975.

[27] Isakowitz, S. J., "International reference guide to space launch systems," *NASA STI/Recon Technical Report A*, Vol. 91, 1991, p. 51425.

[28] Mc Bride, B., Reno, M., and Gordon, M., "CET93 and CETPC: An Interim Updated Version of the NASA Lewis Computer Program for Calculating Complex Chemical Equilibria With Applications," NASA TM-4557, NASA, March 1994.

[29] Barrere, M., Jaumotte, A., De Veubeke, B. F., and Vandenkerckhove, J., *Rocket Propulsion*, Elsevier Publishing Company, Amsterdam, The Netherlands, 1960.

[30] Barker, D., Kording, J., Belnap, R., and Hall, A., "A Simplified Method of Predicting Char Formation in Ablating Rocket Exit Cones," *AIChE Chemical Engineering Progress Symposium Series*, Vol. 61, 1965, pp. 108–114.

[31] Casalino, L., and Pastrone, D., "Optimal Design of Hybrid Rocket Motors for Microgravity Platform," *Journal of Propulsion and Power*, Vol. 24, No. 3, 2008, pp. 491–498. doi:10.2514/1.30548.

[32] Casalino, L., Colasurdo, G., and Pastrone, D., "Optimal Low-Thrust Escape Trajectories Using Gravity Assist," *Journal of Guidance, Control, and Dynamics*, Vol. 22, No. 5, 1999, pp. 637–642. doi:10.2514/2.4451.

[33] Rosa Sentinella, M., and Casalino, L., "Hybrid Evolutionary Algorithm for the Optimization of Interplanetary Trajectories," *Journal of Spacecraft and Rockets*, Vol. 46, No. 2, 2009, pp. 365–372. doi:10.2514/1.38440.

[34] Haimes, Y., Lasdon, L., and Wismer, D., "On a Bicriterion Formation of the Problems of Integrated System Identification and System Optimization," *IEEE Transactions on Systems, Man and Cybernetics*, , No. 3, 1971, pp. 296–297. doi: 10.1109/TSMC.1971.4308298.

[35] Colasurdo, G., and Pastrone, D., "Indirect Optimization Method for Impulsive Transfer," Paper AIAA-94-3762, AIAA, 1994. doi:10.2514/6.1994-3762.

[36] Stark, R. H., "Flow separation in rocket nozzles-an overview," Paper AIAA 2013-3840, AIAA, 2013. doi:10.2514/6.2013-3840.